THE JOURNAL OF PHYSICAL CHEMISTRY A

ARTICLE

pubs.acs.org/JPCA

# Electron Spin Multiplicities of Transition-Metal Aromatic Radicals and Ions: $M[C_6(CH_3)_6]$ and $M^+[(C_6(CH_3)_6]$ (M = Ti, V, and Co)

Jung Sup Lee, Yuxiu Lei, and Dong-Sheng Yang*

Department of Chemistry, University of Kentucky, Lexington, Kentucky 40506-0055, United States

Supporting Information

**ABSTRACT:** Determination of electron spin multiplicities of transition-metal radicals and ions challenges both experimentalists and theoreticians. In this work, we report preferred electron spin states of $M[C_6(CH_3)_6]$ and $M^+(C_6(CH_3)_6]$, where M = Ti, V, and Co. The neutral radicals were formed in a supersonic metal cluster beam source, and their masses were measured with time-of-flight mass spectrometry. Precise ionization energies of the radicals and metal−ligand stretching frequencies of the ions were measured by pulsed field ionization zero electron kinetic energy spectroscopy. C−H stretching frequencies of the methyl group in the radicals were obtained by infrared−ultraviolet two-photon ionization. Electron spin multiplicities of the radicals and ions were investigated by combining the spectroscopic measurements, density functional theory, and Franck−Condon factor calculations. The preferred spin states are quintet, sextet, and quartet for the neutral Ti, V, and Co radicals, respectively; for the corresponding singly charged cations, they are quartet, quintet, and triplet. In these high-spin states, the aromatic ring remains nearly planar. This finding contrasts to the previous study of Sc(hmbz), for which low-spin states are favored, and the aromatic ring is severely bent.

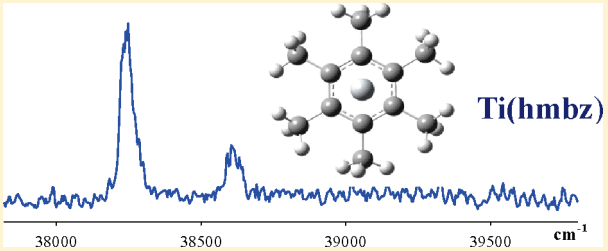


## 1. INTRODUCTION

Interactions between transition-metal atoms and aromatic molecules play fundamental roles in homogeneous catalysis involving C−C and C−H bond activation[1−3] and hydrogenation.[4−6] Although there have been numerous experimental and computational studies of metal−benzene complexes,[7] electron spin multiplicities of the monobenzene species are still under debate. For Ti(benzene), both triplet[8,9] and quintet[10−16] states have been predicted as the ground electronic state, and the electron spin preferences appeared to depend on computational methods. For instance, B3LYP calculations predicted the quintet state to be the ground state with the triplet state lying <1 kcal $mol^{-1}$ above, while the BPW91 method yielded the triplet ground state with the quintet state at 4 kcal $mol^{-1}$ higher in energy.[8] The electric dipole moment of Ti(benzene) was determined to be 2.4 ± 0.3 D via the measurement of the complex intensity as a function of the electrostatic hexapole field.[13] Because the electric dipole moments of the triplet and quintet states were predicted to be close to each other (2.85 ± 0.12 D), the comparison of the experimental and theoretical dipole moments was unable to distinguish the two spin states. For V(benzene), doublet,[15,17−20] quartet,[19] or sextet[10] states have been predicted to be the ground state. The spin multiplicity of V(benzene) is not only sensitive to the computational methods but also to the basis sets.[15,19] For example, the BPW91 calculations yielded a spin quartet ground state with the Lanl2dz basis and a spin doublet ground state with the 6-311G** basis.[19] On the other hand, a doublet ground state has been proposed from matrix-isolation infrared and electron spin resonance spectroscopic studies.[17,18,20,21] For Co(benzene), previous theoretical calculations have predicted a doublet ground state.[10,12,22] For singly charged positive ions, theoretical calculations have predicted a quartet ground state for $Ti^+$(benzene),[9,10,23−26] quintet[10,23−25] or triplet[25,27] for $V^+$-(benzene), and a triplet for $Co^+$(benzene).[23−25] For $V^+$-(benzene), where two possible spin states were predicted, vibrational photodissociation spectra suggested that the ground state might be the high-spin quintet.[7,26,28,29]

In the present study, electron spin multiplicities of $M[(C_6(CH_3)_6]$ and $M^+[C_6(CH_3)_6]$ (M = Ti, V, and Co) are examined by comparing spectroscopic measurements and theoretical calculations. The spectroscopic measurements include single-photon pulsed field ionization zero electron kinetic energy (ZEKE) and IR−UV resonant two-photon ionization. The theoretical calculations consist of the predictions of the low-energy electronic states by density functional theory (DFT) and the spectral simulations on the basis of the Franck−Condon (FC) principle. Because the metal binding with methylated benzenes is generally stronger than that with benzene,[30] the benzene methylation enhances the production of the monoligand metal complexes and thus facilitates the ZEKE or IR−UV measurements on these metal−aromatic species.

## 2. EXPERIMENTAL AND COMPUTATIONAL METHODS

**A. Single-Photon ZEKE Spectroscopy.** The molecular beam ZEKE spectrometer used in this work has been described in a

**Received:** March 21, 2011
**Revised:** May 10, 2011
**Published:** May 19, 2011

previous publication.[31] The M[$C_6(CH_3)_6$] (M = Ti, V, and Co) complexes were synthesized by reactions of metal atoms with the vapor of hexamethylbenzene (hmbz) (99%, mp 165−168 °C, TCI America) in a laser vaporization cluster beam source. The metal atoms were produced by laser ablation of a metal rod (Ti, 99.7%; V, 99.7%; and Co, 99.95%; Aldrich) with the second-harmonic output of a pulsed neodymium-doped yttrium aluminum garnet (Nd:YAG) laser (Continuum Minilite II, 532 nm, 3−5 mJ) in the presence of He, Ar, or a He/Ar mixture (ultra-high-purity, Scott−Gross). These gases were delivered by a homemade piezoelectric pulsed valve with a backing pressure of 40−70 psi.[32] The metal rod was translated and rotated by a motor-driven mechanism to ensure that each laser pulse ablated a fresh metal surface. The ligand was placed in a small copper oven inside of the vacuum chamber and heated to 37 °C for Ti(hmbz) and V(hmbz) but kept at room temperature for Co(hmbz). The vapor of the ligand interacted with the metal atoms entrained in the carrier gas to form the metal complexes, which were then expanded into the vacuum through the pulsed valve nozzle. The molecular beams were collimated by a cone-shaped skimmer (4 mm i.d.) and passed through a pair of charged deflection plates (+500 V) to remove residual ionic species that might have been formed by laser ablation.

Prior to ZEKE measurements, the production of the metal complexes was maximized by optimizing the timing and power of the vaporization and ionization lasers, the backing pressure of the carrier gas, and the amount of the ligand vapor. The neutral metal complexes in molecular beams were ionized by a frequency-doubled dye laser (Lumonics HD-500) pumped by the third-harmonic output of a second pulsed Nd:YAG laser (Continuum Surelite II, 355 nm) and identified by photoionization time-of-flight mass spectrometry. Ionization thresholds of the complexes were located from threshold photoionization efficiency (PIE) spectra, which present the mass-selected ion signal as a function of the ionization laser wavelength. The ZEKE electrons were produced by photoexcitation of the neutral complexes to highly excited Rydberg states, followed by pulsed field (3 $\mu$s in time delay, 1.2 V $cm^{-1}$ in field strength, and 100 ns in pulse width) ionization of the high-energy Rydberg molecules. A small dc field (0.06 V $cm^{-1}$) was applied to discriminate the ZEKE electrons from the kinetic electrons produced by direct photoionization. A delay pulse generator (Stanford Research Systems DG535) was used to generate the pulsed electric field for ionization. The ion and electron signals were detected by a dual microchannel plate detector (Galileo), amplified by a preamplifier (Stanford Research Systems SR445), averaged by a gated integrator (Stanford Research Systems SR250), and stored in a laboratory computer. Laser wavelengths were calibrated against vanadium or titanium atomic transitions.[33] The dc field effects on the PIE and ZEKE spectral energies were corrected using the relation of $\Delta IE = 6.1E_F^{1/2}$, where $E_F$ in V $cm^{-1}$ is the field strength.[34]

**B. IR−UV Photoionization Spectroscopy.** Details of IR−UV two-photon ionization spectroscopy have been described in a previous publication.[35] An IR optical parametric oscillator/amplifier (OPO/A) laser (LaserVision) was used for vibrational excitation and a frequency-doubled UV dye laser (Lumonics HD-500) for molecular ionization. The IR OPO/A laser was pumped by a Nd:YAG laser (Continuum Surelite III) with the injection seeder off, and the dye laser was pumped by a Nd:YAG laser (Continuum Surelite II). The IR and UV laser beams were counterpropagated, and both were perpendicular to the molecular beam. The time difference between the IR and UV lasers was in the range of 50−200 ns. The UV laser was fixed at 150−200 $cm^{-1}$ below the ionization energy (IE) of the metal complexes, and the IR laser was scanned in the C−H stretch region. The $M^+$(hmbz) ion signal was detected in the same time-of-flight spectrometer as that used in the ZEKE experiment. The IR laser wavelengths were calibrated with the photoacoustic spectra of $H_2O$.[36]

**Table 1. Point Groups, Electronic States, Electronic Energies ($E_{rel}$, $cm^{-1}$), and Adiabatic Ionization Energies (AIEs, $cm^{-1}$) of M(hmbz) (M = Ti, V, and Co; hmbz = hexamethylbenzene) from B3LYP/6-311+G(d,p) Calculations**

| complexes | symmetry | states | $E_{rel}$ ($cm^{-1}$) | transitions | AIE ($cm^{-1}$) |
|---|---|---|---|---|---|
| Ti(hmbz) | | | | | 38248(5)[a] |
| | $C_s$ | $^2A''$ | 44184 | $^2A'' \leftarrow {}^1A'$ | 37766 |
| | $C_1$ | $^4A$ | 36939 | $^2A'' \leftarrow {}^3A_2$ | 42573 |
| | $C_s$ | $^1A'$ | 6596 | $^4A \leftarrow {}^3A_2$ | 35654 |
| | $C_{2v}$ | $^3A_2$ | 1761 | $^4A \leftarrow {}^5A$ | 37244 |
| | $C_1$ | $^5A$ | 0 | | |
| V(hmbz) | | | | | 40364(10)[a] |
| | $C_s$ | $^1A'$ | 46754 | $^1A' \leftarrow {}^2A_1$ | 44848 |
| | $C_s$ | $^3A''$ | 39228 | $^3A'' \leftarrow {}^2A_1$ | 37406 |
| | $C_1$ | $^5A$ | 37087 | $^3A'' \leftarrow {}^4B_2$ | 38202 |
| | $C_{2v}$ | $^2A_1$ | 2139 | $^5A \leftarrow {}^4B_2$ | 36104 |
| | $C_{2v}$ | $^4B_2$ | 1273 | $^5A \leftarrow {}^6A$ | 37402 |
| | $C_1$ | $^6A$ | 0 | | |
| Co(hmbz) | | | | | 40807(5)[a] |
| | $C_2$ | $^1A$ | 51802 | $^1A \leftarrow {}^2B$ | 48829 |
| | $C_s$ | $^3A''$ | 38979 | $^3A'' \leftarrow {}^2B$ | 36093 |
| | $C_2$ | $^2B$ | 3397 | $^3A'' \leftarrow {}^4A''$ | 39290 |
| | $C_s$ | $^4A''$ | 0 | | |

[a] From ZEKE measurements.

**C. Computation.** Molecular geometries, vibrational frequencies, and IR intensities of the neutral and ionized metal complexes were obtained from B3LYP/6-311+G(d,p) calculations.[37] The B3LYP/6-311+G(d,p) method was selected because it has yielded reasonable predictions of IEs, vibrational frequencies, and spectral intensities of metal−aromatic complexes.[30,38−43] To simulate the ZEKE spectra, multidimensional FC factors were calculated from the equilibrium geometries, harmonic vibrational frequencies, and normal coordinates of the neutral and ionized complexes.[44,45] The Duschinsky effect[46] was considered to account for the normal mode differences between the neutral and ionic complexes in the FC calculations. A Lorentzian band shape with the experimental band width was used to simulate the spectral broadening. ZEKE transition intensities from excited vibrational levels of the neutral complexes were calculated by assuming thermal excitation at specific temperatures. The C−H stretching frequencies were scaled by a factor of 0.9670, the averaged ratio of the measured to predicted C−H stretching frequencies of the free ligand.[47] The IR intensities of C−H stretches were calculated from the first derivative of the dipole moment at the equilibrium bond distance, and the IR spectra were plotted with the experimental band width.

## 3. RESULTS AND DISCUSSION

**A. Predicted Low-Energy Electronic States and Benzene Ring Deformation.** Table 1 summarizes the low-energy electronic

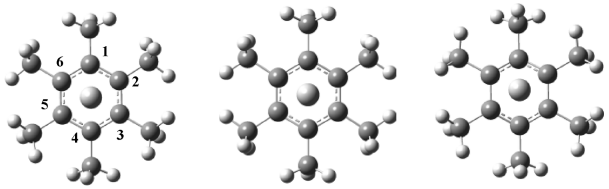

(a) Ti(hmbz)

| Symm | $C_1$ | $C_{2v}$ | $C_s$ |
|---|---|---|---|
| State | $^5$A/$^4$A | $^3$A$_2$ | $^1$A'/$^2$A" |

(b) V(hmbz)

| Symm | $C_1$ | $C_{2v}/C_s$ | $C_{2v}/C_s$ |
|---|---|---|---|
| State | $^6$A/$^5$A | $^4$B$_2$/$^3$A" | $^2$A$_1$/$^1$A' |

(c) Co(hmbz)

| Symm | $C_s$ | $C_2$ |
|---|---|---|
| State | $^4$A"/$^3$A" | $^2$B/$^1$A |

**Figure 1.** The minimum-energy conformers of M(hmbz) (M = Ti, V, and Co; hmbz = hexamethylbenzene) in various neutral/ion electronic states. Methyl group orientations are different among different electron spin states.

states of M(hmbz) and $M^+$(hmbz) (M = Ti, V, and Co) and the adiabatic IEs of possible ionization processes of the neutral complexes from B3LYP/6-311+G(d,p) calculations. Because Ti ([Ar]3d$^2$4s$^2$, $^3$F), V ([Ar]3d$^3$4s$^2$, $^4$F), and Co ([Ar]3d$^7$4s$^2$, $^4$F) atoms have four, five, and nine valence electrons, we considered the electron spin multiplicities of 1, 3, 5 for Ti(hmbz); 2, 4, and 6 for V(hmbz); and 2 and 4 for Co(hmbz). With the removal of an electron by ionization, the spin multiplicities of the singly charged $M^+$(hmbz) ions are 2 and 4, 1, 3, and 5, and 1 and 3 for M = Ti, V, and Co, respectively. For all three neutral complexes, high-spin electronic states are predicted to be lower in energy than the low-spin states. However, the energy differences between the low- and high-spin states are very small, especially for the Ti and V species. For example, the differences are only 0.15 and 0.11 eV between the $^6$A and $^4$B$_2$ states or the $^4$B$_2$ and $^2$A$_1$ states of V(hmbz). Because these spin states are close to each other, theory alone is problematic in determining the ground states of these species.

Although the energy differences between the various spin states are small, their geometric variations are rather large. First, the orientations of the methyl groups are different among the spin states, as shown in Figure 1. For the highest spin states [i.e., $^5$A ($C_1$) of Ti(hmbz), $^6$A ($C_1$) of V(hmbz), and $^4$A″ ($C_s$) of Co(hmbz)], all three pairs of the *para*-methyl groups are each in a staggered configuration, as in the case of the free ligand;[48−50] for the other spin states, two pairs of the *para*-methyl groups are staggered, and one pair is eclipsed. Second, the degree of the benzene ring distortion caused by metal coordination varies significantly among the three complexes and different spin states of each species, as displayed in Figure 2. The ring dihedral angels (∠C−C−C−C) are in the 4.2−23.8° range for Ti(hmbz), 10.8−21.7° for V(hmbz), and 2.2−4.3° for Co(hmbz). A large ring deformation is predicted for the low-spin states, that is, $^1$A′ ($C_s$) of Ti(hmbz) and $^2$A$_1$/ $^4$B$_2$ ($C_{2v}$) of V(hmbz). Although the six ring C−C bond lengths (1.406 Å) are the same in free hmbz, the ring C−C bond distances (Table S1 in the Supporting Information) are rather different in these low-spin states (i.e,

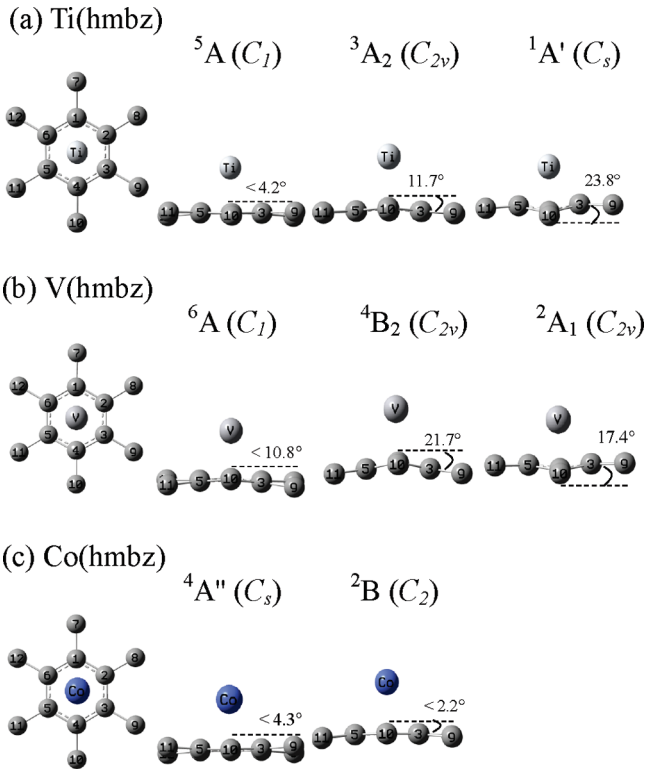


**Figure 2.** Conformations of the M(hmbz) (M = Ti, V, and Co; hmbz = hexamethylbenzene) complexes in various electron spin states. The dihedral angles are for ∠$C_2$−$C_3$−$C_4$−$C_5$, and hydrogen atoms are omitted in the figure.

1.416/1.476 in $^1$A′ of Ti(hmbz) and 1.396/1.471 Å in $^4$B$_2$ of V(hmbz)). The C−C bond distances in these states are close to the averaged ring C−C double and single bond lengths (1.375/1.462 Å) in the transition-metal arene compounds, where the arene ligands are distorted to 1,4-dienes.[51] Thus, the $\pi$ electrons in these Ti(hmbz) and V(hmbz) low-spin states are significantly localized because of the severe ring deformation. In contrast, small ring deformation is predicted for the high-spin states, that is, $^5$A ($C_1$) of Ti(hmbz) and $^4$A″ ($C_s$) of Co(hmbz). In each of these states, the six ring C−C bond lengths are about the same. The almost identical C−C bond distances and nearly planar ring indicate that the $\pi$ electrons in these states are still largely delocalized among the six ring C atoms. The distinct ring deformation for different spin states has also been found for Sc(hmbz), where the benzene ring is severely distorted in the low-spin doublet but nearly planar in the high-spin quartet states.[30] Ionization removes an electron from the neutral complexes and yields the singly charged ions in various spin states, with high-spin states being more stable (Table 1). Like the neutral states, the low-spin states of the cations exhibit significantly more distortion for the benzene ring than the high-spin states (Table S1, Supporting Information).

**B. Spectroscopy and Preferred Electron Spin States.** *(1). PIE Spectra of M(hmbz) (M = Ti, V, and Co).* Figure 3 presents the PIE spectra of the M(hmbz) complexes seeded in He carrier. Each spectrum exhibits a sharp onset of the ion signal. The energy of the onset corresponds to the ionization threshold of each complex and can be estimated from the intersecting point of two lines drawn through a baseline and a sharp signal rising line, as indicated by the arrows in the figure. The estimated thresholds


dx.doi.org/10.1021/jp202666u |*J. Phys. Chem. A* 2011, 115, 6509–6517

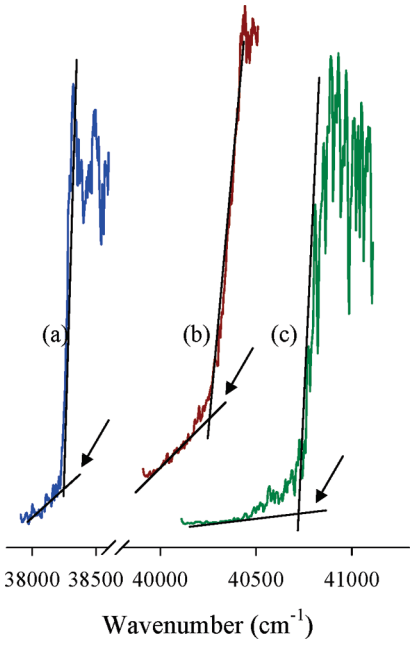


**Figure 3.** PIE spectra of M(hmbz) (M = Ti (a), V (b), and Co (c); hmbz = hexamethylbenzene) seeded in He carrier. The ionization threshold of each complex is estimated from the intersection point of the baseline and ion signal rising onset, as indicated by the arrows.

are 38220 (50), 40300 (100), and 40770 (50) $cm^{-1}$ for the Ti, V, and Co complexes, respectively. These values are corrected by adding the energy shift of +110 $cm^{-1}$ to the laser wavenumbers to account for the dc extraction field effect (320 $Vcm^{-1}$) in the ionization region.[34] The measurement of the PIE spectra is used to simplify the search for and correlate with the ZEKE electron signal.

*(2). ZEKE Spectra and Electron Spin States of Ti(hmbz) and V(hmbz).* Figures 4a and 5a show ZEKE spectra of Ti(hmbz) and V(hmbz) seeded in He carrier. The spectra of the two complexes are simple, each with only two bands. The first band and the band separation of Ti(hmbz) are measured to be 38248 and 356 $cm^{-1}$, whereas those of V(hmbz) are 40364 and 392 $cm^{-1}$, respectively. The energy position of the first band correlates with the ionization threshold measured from the PIE spectrum (with a much smaller uncertainty) and corresponds to the adiabatic IE of the individual complex. The band separations in the two complexes are comparable to the stretching frequencies of $Sc^+$−benzene (375 $cm^{-1}$)[38] and $Sc^+$−hmbz (400 $cm^{-1}$)[30] and can be assigned to the excitation of $Ti^+$−hmbz or $V^+$−hmbz stretching vibrations. In addition to these bands, the spectrum of V(hmbz) displays a sharp line at 40556 $cm^{-1}$, as marked by the asterisk in Figure 5a. This sharp line arises from a V atomic transition ($^2p^o_{3/2} \leftarrow {}^4F_{5/2}$).[33] The ZEKE bands are relatively broad, ~50 $cm^{-1}$ for Ti(hmbz) and ~100 $cm^{-1}$ for V(hmbz). The broad spectra are due to unresolved transitions from excited rotational and vibrational levels of the neutral complexes. Transitions from additional rotational isomers with different methyl orientations may be possible; however, no other local minima with different methyl orientations are located, except for those presented in Figure 1. Attempts to record spectra at lower temperatures (i.e., with heavier carrier gases) failed for these two species.

To investigate the electronic transitions contributing to the ZEKE spectra, the measured spectra are compared with the

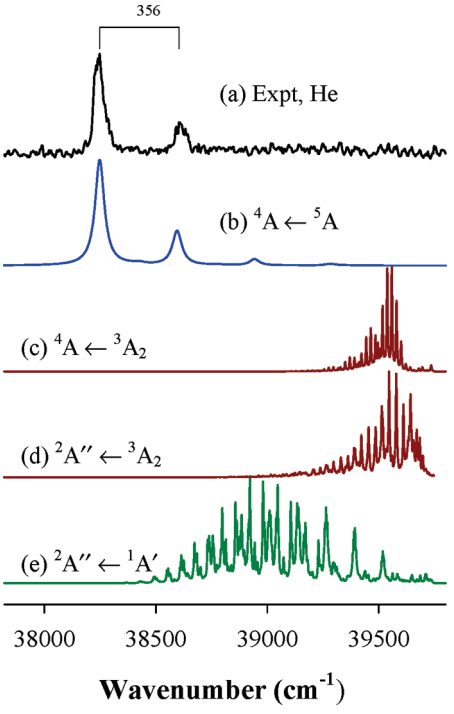


**Figure 4.** Experimental ZEKE spectrum of Ti(hmbz) seeded in He (a) and simulations of the $^4A \leftarrow {}^5A$ (b), $^4A \leftarrow {}^3A_2$ (c), $^2A'' \leftarrow {}^3A_2$ (d), and $^2A'' \leftarrow {}^1A'$ (e) transitions at 10 K.

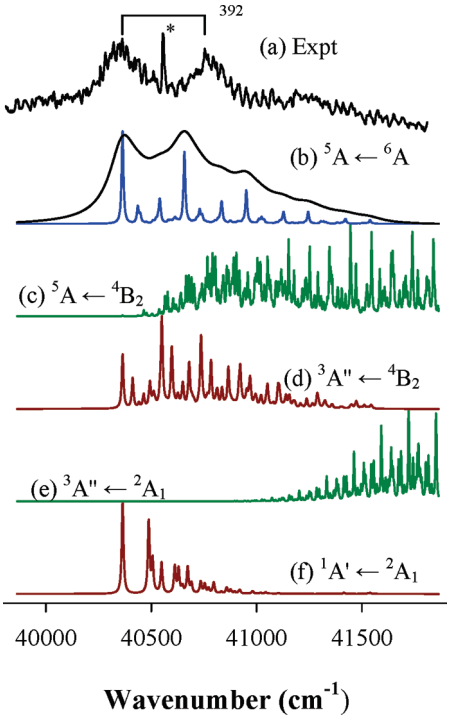


**Figure 5.** ZEKE spectrum of V(hmbz) seeded in He (a) and simulations of the $^5A \leftarrow {}^6A$ (b), $^5A \leftarrow {}^4B_2$ (c), $^3A'' \leftarrow {}^4B_2$ (d), $^3A'' \leftarrow {}^2A_1$, and $^1A' \leftarrow {}^2A_1$ (e) transitions at 10 K.

spectral simulations of all possible transitions (Figures 4 and 5). In these simulations, the theoretical vibrational frequencies are not scaled, but the predicted IE energies are shifted to the

experimental values for clear comparison. For Ti(hmbz), the simulation of the $^4A \leftarrow {}^5A$ transition (Figure 4b) matches nicely to the experimental spectrum. The predicted IE (37244 $cm^{-1}$) and $Ti^+$−hmbz stretching frequency (347 $cm^{-1}$) agree with the measured values (38248 and 356 $cm^{-1}$), and the $^5A$ state is predicted to be the ground state of the neutral complex (Table 1). The simple spectrum with a very short $Ti^+$−hmbz stretching progression indicates that ionization causes only a small geometry change by removing a Ti-based electron. Indeed, the M−C and C−C distances and the benzene ring dihedral angles of the $^5A$ neutral state are rather similar to those of the $^4A$ ion state (Table S1, Supporting Information). The agreement between the theory and experiment shows that the $^4A \leftarrow {}^5A$ transition is responsible for the observed spectrum, and Ti(hmbz) and $Ti^+$(hmbz) prefer the quintet and quartet spin states, respectively. All other transitions (i.e., $^4A \leftarrow {}^3A_2$, $^2A'' \leftarrow {}^3A_2$, and $^2A'' \leftarrow {}^1A'$) are not involved in the ZEKE spectrum because they exhibit different IEs, long FC profiles, and mismatched vibrational intervals. The long FC profiles are due to large structural changes from the neutral state to the ion state (Table S1, Supporting Information). The lack of the contributions from the transitions of the low-spin states is not surprising because the $^1A'$ and $^3A_2$ neutral states are excited states (i.e., 1761 and 6596 $cm^{-1}$ above the $^5A$ ground state, respectively) and are expected to be quenched by the supersonic cooling.

Similar to Ti(hmbz), simulations from transitions of lower spin states (i.e., $^5A \leftarrow {}^4B_2$, $^3A'' \leftarrow {}^4B_2$, $^3A'' \leftarrow {}^2A_1$, and $^1A' \leftarrow {}^2A_1$) do not agree with the experimental spectrum; the FC profiles in the $^5A \leftarrow {}^4B_2$ and $^3A'' \leftarrow {}^2A_1$ transitions (Figure 5c,e) are too long with negligible 0−0 band intensity, while the vibrational intervals in the $^3A'' \leftarrow {}^4B_2$ and $^1A' \leftarrow {}^2A_1$ transitions (Figure 5d,f) are too small. The best match to the experimental spectrum is the simulation of the $^5A \leftarrow {}^6A$ transition (Figure 5b). In this transition, the most active vibrational mode is predicted to be the $V^+$−hmbz stretch, and two other modes of weak intensities are methyl torsions. The transitions from these vibrational modes are presented in the lower trace of Figure 5b. If each of the transitions is plotted with the experimental line width (upper trace), the simulation resembles the experimental spectrum, where the weak transitions from the low-frequency torsional modes are unresolved and embedded in the strong $V^+$−hmbz stretching bands. From the $^5A \leftarrow {}^6A$ simulation, the 392 $cm^{-1}$ interval is assigned to the $V^+$−hmbz stretching frequency, consistent with the assignment obtained by comparing the V(hmbz) spectrum with the spectra of Sc(hmbz)[38] and Ti(hmbz) discussed above. The $^6A$ state is predicted to be the ground state, in line with the assignment of the $^5A \leftarrow {}^6A$ transition to the observed spectrum. As in the case of Ti/$Ti^+$(hmbz), the highest-spin state of V/$V^+$(hmbz) ($^6A/{}^5A$) suffers the smallest benzene ring deformation among all spin states. It should be noted that the predicted $V^+$−hmbz stretching frequency (294 $cm^{-1}$) is significantly smaller than the measured value (392 $cm^{-1}$). This is different from the Ti complex, where the calculated $Ti^+$−hmbz stretching frequency (347 $cm^{-1}$) is in excellent agreement with the experimental value (356 $cm^{-1}$). We also calculated $V^+$(hmbz) vibrational frequencies of the $^5A$ state by using DFT/B3P86 and MP2 methods. Unfortunately, both B3P86 and MP2 methods yielded similar $V^+$−hmbz stretching frequencies of around 300 $cm^{-1}$.

*(3). ZEKE and IR−UV Ion Spectra and Electron Spin States of Co(hmbz).* Figure 6 presents the spectra of Co(hmbz) seeded in He, He/Ar, and Ar carriers. Similar to the Ti and V complexes, the spectra are rather broad with He but become sharper with increasing mass of the carrier gas. The spectral line width is reduced from ~80 $cm^{-1}$ in He to 4 $cm^{-1}$ in Ar; the sharp spectrum results from the efficient cooling of the Ar supersonic jet.[52] Because of the narrow line width, the spectrum with Ar exhibits many more resolved transitions, including five vibrational intervals (416, 359, 43, 17, and 20 $cm^{-1}$; see Figure 7a). Additionally, there are two sharp peaks (41645 and 41785 $cm^{-1}$, marked by asterisks) in the spectra with all three carrier gases. The intensity of these peaks strongly depended on the laser power, and they are due to atomic transitions from two-photon excitation.

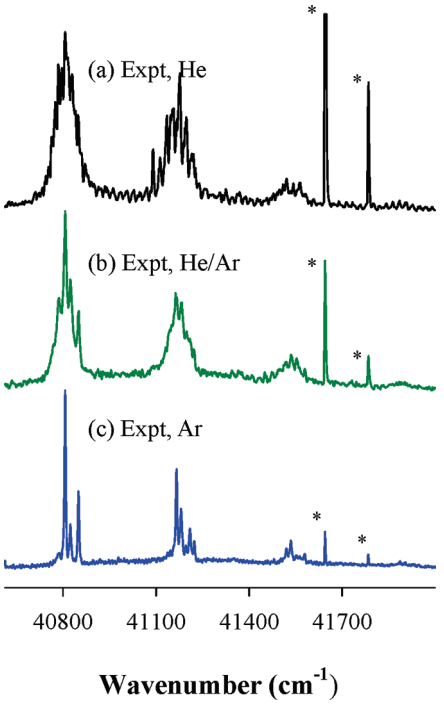


**Figure 6.** Experimental ZEKE spectra of Co(hmbz) seeded in He (a), a He/Ar 1:1 mixture (b), and Ar (c) carrier gases.

Two of the observed vibrational intervals can be assigned by comparing with the vibrational frequencies of the free ligand[53] or with the ZEKE spectra of M(hmbz) (M = Sc,[30] Ti, and V). The 416 $cm^{-1}$ interval is close to the C−$CH_3$ bending frequencies of the free ligand (406, 411, and 451 $cm^{-1}$) measured by inelastic neutron scattering.[53] Among the three C−$CH_3$ bending vibrations, only the 411 $cm^{-1}$ mode is totally symmetric. Thus, the 416 $cm^{-1}$ vibration in the ZEKE spectrum of Co(hmbz) likely corresponds to the 411 $cm^{-1}$ mode in the free ligand. The 359 $cm^{-1}$ interval of the major progression is comparable to those of the $Sc^+$−hmbz (400 $cm^{-1}$), $Ti^+$−hmbz (356 $cm^{-1}$), and $V^+$−hmbz (392 $cm^{-1}$) stretching frequencies and is thus assigned to the $Co^+$−hmbz stretching excitation.

Similar to Ti(hmbz) and V(hmbz), the high-spin electronic state ($^4A''$, $C_s$) of Co(hmbz) is predicted to be more stable than the low-spin doublet state ($^2B$, $C_{2v}$) (Table 2). The transition energy of $^3A'' \leftarrow {}^4A''$ (39290 $cm^{-1}$) is close to the measured IE value (40807 $cm^{-1}$), while the transition energies of $^1A \leftarrow {}^2B$ (48829 $cm^{-1}$) or $^3A'' \leftarrow {}^2B$ (36093 $cm^{-1}$) are either too high or too low compared to the experimental value. Figure 7b−d shows the spectral simulations of the $^3A'' \leftarrow {}^4A''$, $^3A'' \leftarrow {}^2B$, and $^1A \leftarrow {}^2B$ transitions, in comparison with the measured spectrum

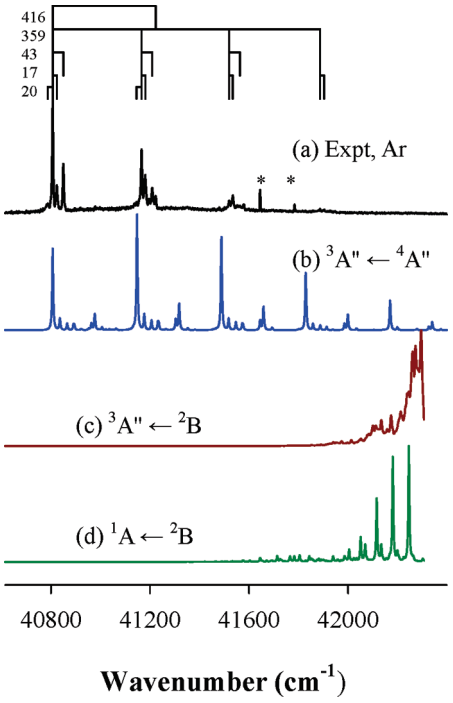


**Figure 7.** ZEKE spectrum of Co(hmbz) seeded in Ar (a) and simulations of the $^3$A″ ← $^4$A″ (b), $^3$A″ ← $^2$B (c), and $^1$A ← $^2$B (d) transitions at 10 K.

(Figure 7a). It is clear that the $^3$A″ ← $^2$B and $^1$A ← $^2$B simulations exhibit FC profiles that are too long compared to the experimental spectrum. On the other hand, the $^3$A″ ← $^4$A″ simulation reasonably reproduces the overall features of the experimental spectrum. The major progression in this simulation has the vibrational interval of 341 cm$^{-1}$, which matches nicely to the experimental progression of 359 cm$^{-1}$. The predicted 412 cm$^{-1}$ vibration is in excellent agreement with the measured 416 cm$^{-1}$ interval. The simulation also reproduces the satellite peaks in the experimental spectrum. On the basis of the good agreement between the simulation and experiment, the observed 416, 359, 43, and 17 cm$^{-1}$ intervals are assigned to a C−CH$_3$ bend, a Co$^+$−hmbz stretch, and CH$_3$ asymmetric and symmetric torsions, respectively, in the $^3$A″ ion state, and the 20 cm$^{-1}$ interval is attributed to the CH$_3$ asymmetric torsion in the $^4$A″ neutral state (Table 2). The assignments of 416 cm$^{-1}$ to the C−CH$_3$ bend and 359 cm$^{-1}$ to the Co$^+$−hmbz are consistent with those from the comparison with the free ligand and other metal complexes discussed above.

To further support the observed $^4$A″ neutral state, we also measured ion spectra by IR−UV two-photon ionization. Compared to the Ti and V complexes, we were able to produce a higher density of the Co(hmbz) complex in the molecular beam. The high density of the Co complex was reflected in the photoionization mass spectra and made it possible to record two-photon ionization ion spectra. In this method, the UV laser wavelength was fixed at 40600 cm$^{-1}$ (∼200 cm$^{-1}$ below the IE of the complex), and the IR laser wavelength was scanned in the range of 2700−3200 cm$^{-1}$ to search for C−H stretching vibrations of the complex. The ion spectrum shown in Figure 8a exhibits two groups of transitions in the C−H stretching region, one group at ∼2900 cm$^{-1}$ and the other at ∼3000 cm$^{-1}$. This observation is consistent with the structural feature of the CH$_3$ groups in hmbz. In each CH$_3$ group, the three C−H bonds can be divided into two sets; one C−H bond is in the plane of the benzene ring, and the other two symmetry-equivalent C−H bonds (labeled as C−H$_2$ hereafter) are located above and below the plane. For the free ligand,[47] a C−H stretching frequency was measured at ∼2890 cm$^{-1}$, and a C−H$_2$ stretching was found at ∼3020 cm$^{-1}$. Thus, the transitions of ∼2900 and ∼3000 cm$^{-1}$ in Co(hmbz) should be assigned to the C−H and C−H$_2$ stretching excitations as well. Figure 8b,c shows the calculated IR spectra of the $^4$A″ and $^2$B states. The theoretical C−H stretching frequencies are scaled by an average ratio (0.9670) of the measured to calculated frequencies of the C−H stretching modes in the free ligand. The IR spectrum of the $^4$A″ state clearly shows two sets of transitions that are similar to the observed spectrum, while that of the $^2$B state exhibits three bands with roughly even separations. Thus, the experimental spectrum is assigned to the C−H stretching excitations of the $^4$A″ state, consistent with the conclusion from the ZEKE experiment. For the lower-frequency group in the experimental spectrum, the 2874, 2890, and 2916 cm$^{-1}$ bands are attributed to the symmetric and asymmetric C−H stretching modes (i.e., the stretching of the unique C−H bonds in the CH$_3$ groups attached to the ring carbon atoms of C1, C3, and C5; see Figure 1 for the numbering of the ring carbon atoms). The predicted frequencies for these modes are 2915 ($\nu_{10}/\nu_{55}$) and 2916 ($\nu_9$) (Table 2). Because the calculated frequencies are nearly degenerate, the three transitions appear to be a single band in the simulation. The IR band at 2928 cm$^{-1}$ is assigned to the asymmetric stretches of the unique C−H bonds in the CH$_3$ groups that are attached to the C2, C4, and C5 ring carbon atoms; the calculated frequency for this vibration is 2927 cm$^{-1}$ ($\nu_8/\nu_{54}$) and is in excellent agreement with the measured value. For the higher-frequency group, the 2981 and 3005 cm$^{-1}$ bands are assigned to the symmetric and asymmetric C−H$_2$ stretching. The calculated frequencies for these stretches are 2994 ($\nu_6$), 3021 ($\nu_{50}$), and 3022 ($\nu_2$) cm$^{-1}$, which are in very good agreement with the measured values.

Previously, we reported the IR−UV photoionization ion spectra of Sc(hmbz),[30] which show only a broad band at 2850 cm$^{-1}$. Compared to Sc(hmbz), the C−H stretching modes in Co(hmbz) are better resolved, and their frequencies are blue-shifted by 20−70 cm$^{-1}$. Furthermore, the C−H stretching frequencies of Co(hmbz) are similar to those (∼2900−3000 cm$^{-1}$) of the free ligand.[47] These observations indicate that Co coordination has a smaller effect on the C−H coordinates of hmbz than Sc. This differential effect on the C−H coordinates is related to the charge distribution of the carbon atoms in the methyl groups. An atomic charge analysis shows that the charges on the carbon atoms of the methyl groups in Co(hmbz) (−0.77 e) are similar to those of the free ligand (−0.79 e), whereas the charges in Sc(hmbz)(−0.12 e) are much smaller. On the other hand, the charges on the hydrogen atoms are similar in Co(hmbz), Sc(hmbz), and hmbz. Therefore, the C−H bonds are more polarized in Co(hmbz) than those in Sc(hmbz), resulting in stronger C−H bonds and higher C−H stretching frequencies in the Co complex.

*(4). Ionization and Preferred Spin States of M(hmbz).* Although a metal−ligand complex could be ionized by a ligand-centered multiphoton process, ionization of the M(hmbz) complexes is a metal-centered, single-photon process. This is evident from the good correlation between the measured ionization energy shift from the metal atom to the complex and

**Table 2. Adiabatic Ionization Energies (AIEs, $cm^{-1}$), Ionic and Neutral Bond Energies ($D_0^+/D_0$, kcal/mol), and Vibrational Frequencies ($cm^{-1}$) of M(hmbz) (M = Sc, Ti, V, and Co; hmbz = hexamethylbenzene) from ZEKE Spectroscopy and B3LYP/6-311+G(d,p) Calculations**

| | | ZEKE | B3LYP |
|---|---|---|---|
| Sc(hmbz) | AIE | 39535 (5) | 38931 |
| ($C_{2v}$, $^1A_1 \leftarrow {}^2A_1$)[a] | ΔAIE[b] | 13387 | |
| | $D_0$ | | 19.4 |
| | $D_0^+$ | | 59.5 |
| | $Sc^+$−hmbz stretch ($\nu_{21}^+$) | 400 | 366 |
| | C−H stretch ($\nu_{69}$) | 2850[c] | 2861[d] |
| Ti(hmbz) | AIE | 38248 | 37244 |
| ($C_1$, $^4A \leftarrow {}^5A$) | ΔAIE[b] | 16824 | |
| | $D_0$ | | 25.3 |
| | $D_0^+$ | | 66.4 |
| | $Ti^+$−hmbz stretch ($\nu_{74}^+$) | 356 | 347 |
| V(hmbz) | AIE | 40364 (10) | 37402 |
| ($C_1$, $^5A \leftarrow {}^6A$) | ΔAIE[b] | 14047 | |
| | $D_0$ | | 15.3 |
| | $D_0^+$ | | 59.3 |
| | $V^+$−hmbz stretch ($\nu_{75}^+$) | 392 | 294 |
| Co(hmbz) | AIE | 40807 (5) | 39290 |
| ($C_s$, $^3A'' \leftarrow {}^4A''$) | ΔAIE[b] | 22757 | |
| | $D_0$ | | 7.1 |
| | $D_0^+$ | | 72.7 |
| | $CH_3$ asymmetric torsion ($\nu_{86}$/ $\nu_{86}^+$) | 23/43 | 42/57 |
| | $CH_3$ symmetric torsion ($\nu_{47}^+$) | 17 | 29 |
| | $Co^+$−hmbz stretch ($\nu_{41}^+$) | 359 | 341 |
| | C−$CH_3$ bend ($\nu_{38}^+$) | 416 | 412 |
| | symmetric and asymmetric C−H stretch [C(1,3,5)−CH] | 2874[c], 2890[c] | 2915[d] ($\nu_{10}/\nu_{55}$) |
| | | 2916[c] | 2916[d] ($\nu_9$) |
| | asymmetric C−H stretch [C(2,4,6)−CH] | 2928[c] | 2927[d] ($\nu_8/\nu_{54}$) |
| | symmetric C−$H_2$ stretch | 2981[c] | 2994[d] ($\nu_6$) |
| | asymmetric C−$H_2$ stretch | 3005[c] | 3021[d] ($\nu_{50}$) |
| | | | 3022[d] ($\nu_2$) |

[a] From ref 38. [b] ΔAIE = AIE (M) − AIE (M(hmbz)). [c] From IR−UV ion spectra. [d] Scaled by a factor of 0.9670.

predicted bond energy difference between the neutral and ionized species (Table 2) (on the basis of the thermodynamic cycle, IE(M) − IE(M−hmbz) = $D_0^+$(M$^+$−hmbz) − $D_0$-(M−hmbz), where $D_0^+$ and $D_0$ are the neutral and ion bond dissociation energies, respectively). Another important piece of evidence for the removal of a metal-based electron is the observation of the strong metal−ligand stretching activity that accompanies ionization. Because the electron is removed from the metal-based orbital, there is a significant change in the metal−ligand bond length between the neutral and ion ground electronic state. This induces the greatest FC activity in the metal−ligand stretch coordinate. The ejection of the metal-based electron should not be surprising because the IEs of Ti, V, and Cr atoms are lower than that of the methyl-substituted benzene.[54]

The M(hmbz) (M = Ti, V, and Co) complexes prefer high-spin $^5A$, $^6A$, and $^4A''$ states, respectively, whereas Sc(hmbz)[30] favors the low-spin $^2A_1$ state (Table 2). The spin preferences of these complexes may be rationalized by considering the ground states of the metal atoms, 3d ← 4s electron promotion energies, electron Coulomb repulsion, and metal−ligand bond energies. For example, V has the ground state of $3d^34s^2$ ($^4F$), the first excited state of ($3d^44s^1$, $^6D$) at 2112 $cm^{-1}$, and the second excited state of ($3d^44s^1$, $^4D$) at 8413 $cm^{-1}$ (ref 33). The energy difference (2112 $cm^{-1}$) between the ($3d^44s^1$, $^6D$) and ($3d^34s^2$, $^4F$) states can be considered the 3d ← 4s promotion energy. This electron promotion results in the increase of the electron spin multiplicity from 4 to 6. On the other hand, the energy difference (6300 $cm^{-1}$) between the ($3d^44s^1$, $^4D$) and ($3d^44s^1$,$^6D$) states can be thought of as the electron Coulomb repulsion energy that is required to pair up electrons. The electron pairing leads to the decrease of the spin multiplicity from 6 to 4. The predicted V−hmbz bond energy (~5300 $cm^{-1}$, Table 2) is larger than the electron promotion energy but smaller than the coulomb repulsion energy of the V atom. Thus, the stabilization from the V−hmbz interaction overcomes the energy cost for the electron promotion, and V(hmbz) adopts the high-spin sextet state. Similarly, the predicted Ti−hmbz bond energy (~8900 $cm^{-1}$, Tabel 2) is sufficient to overcome the promotion energy ($\Delta E$ = $E$($3d^34s$, $a^5F$) − $E$($3d^24s^2$, $a^3F$) = 6556 $cm^{-1}$),[54] leading the Ti complex to be in the high-spin quintet state. In contrast, the Sc−hmbz bond energy (~6800 $cm^{-1}$, Table 2) is much smaller than the electron promotion energy of Sc atom (i.e., $\Delta E$ = $E$($3d^24s^1$, $^4F$) − $E$($3d^14s^2$, $^2D$) = 11520 $cm^{-1}$) but much larger


dx.doi.org/10.1021/jp202666u |J. Phys. Chem. A 2011, 115, 6509–6517

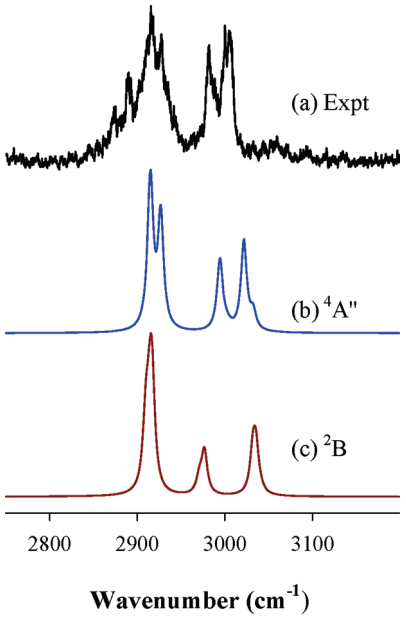


**Figure 8.** Experimental IR−UV photoionization ion spectrum of Co(hmbz) seeded in Ar (a) and simulated IR spectra of the $^4A''$ (b) and $^2B$ (c) states of the complex in the C−H stretching region. The calculated C−H frequencies are scaled by 0.9670, the average ratio of the experimental to the calculated C−H stretching frequencies of the free ligand.

than the energy required to pair up electrons (i.e., $\Delta E$ = $E(3d^24s^1, {}^2F) - E(3d^24s^1, {}^4F) = 3406$ cm$^{-1}$). Thus, Sc(hmbz) is in the low-spin doublet state. For Co(hmbz), the estimated bond energy (~2500 cm$^{-1}$, Table 2) is slightly smaller than both the promotion energy ($\Delta E = E(3d^84s, b^4F) - E(3d^74s^2, a^4F)$ = 3482 cm$^{-1}$) and the coulomb energy ($\Delta E = E(3d^84s, a^2F) - E(3d^84s, b^4F)$ = 3960 cm$^{-1}$). The Co(hmbz) complex is determined to be in the quartet spin state, and the Co electron configuration in the complex ($3d^84s$) is different from that of the bare metal atom ($3d^74s^2$). It may be that the Co−hmbz bond energy is underestimated by theory, which is less than one-half of the bond energies of the other metal (Sc, Ti, and V) complexes.

The benzene ring in the high-spin ground states of the Ti, V, and Co complexes is less perturbed than that in the low-spin ground state of Sc(hmbz), where the benzene ring bending caused by Sc coordination is predicted to be as large as 26.5° (Table S1, Supporting Information). The ring bending degree is associated with the electron occupation of metal valence orbitals in the complexes. Interactions between metal $4s/3d_{z^2}$ and ring-$\pi$ orbitals should have little effect on the ring planarity because the 4s orbital has spherical symmetry and the $3d_{z^2}$ orbital points to the middle of the ring. On the other hand, interactions with other 3d orbitals are expected to affect the ring plane because each of these d orbitals interacts differently with benzene p$\pi$ orbitals. The $d_{x^2-y^2,xy}$ orbitals have a $\delta$ overlap with the empty $\pi_{4,5}$ orbitals and are stabilized by the metal to ligand electron back-donation. The $d_{xz,yz}$ orbitals have a $\pi$ overlap with the filled $\pi_{2,3}$ orbitals and are destabilized by the ligand to metal electron donation or by the filled−filled orbital interaction.[55] If the two d$\delta$ (or d$\pi$) orbitals are unevenly occupied, the aromatic ring plane is expected to be significantly distorted upon metal coordination; otherwise, the ring distortion should be small. For example, in the $^2A_1$ $[(d_{x^2-y^2})^2(sd_{z^2})^1]$ state of Sc(hmbz), the $d_{x^2-y^2}$ orbital is doubly occupied but $d_{xy}$ is empty, resulting in differential d$\delta-\pi$ interactions for the six ring carbon atoms and thus significant ring bending. On the other hand, in the $^5A$ state $[(d_{z^2})^1(d_{xy})^1(d_{x^2-y^2})^1(sd_{z^2})^1]$ of Ti(hmbz), both d$\delta$ ($d_{x^2-y^2}$ and $d_{xy}$) orbitals are singly occupied, and the $\delta-\pi$ interaction is equal for the six carbon atoms. The d$\pi-\pi$ interaction is also equal among the six ring carbons as both $d_{xz}$ and $d_{yz}$ orbitals are unoccupied. This leads to nearly equal Ti−C (2.385 ± 0.002 Å) and C−C (1.428 ± 0.001 Å) distances in the $^5A$ ground state of Ti(hmbz).

## 4. CONCLUSIONS

In this work, we report the first high-resolution electron spectra of M(hmbz) (M = Ti, V, and Co) and IR−UV photoionization ion spectra of Co(hmbz). Precise ionization energies of the three complexes and metal−ligand stretching frequencies of the ions are measured from the electron spectra. C−H stretching frequencies of the methyl groups in the neutral state of Co(hmbz) are determined from the ion spectra. Preferred electron spin multiplicities of the neutral and singly charged ion states are investigated by combining the spectroscopic measurements with DFT and spectral simulations. It is determined that the monoligated complexes prefer high-spin neutral and ionic states, $^5A/^4A$ for Ti/Ti$^+$(hmbz), $^6A/^5A$ for V/V$^+$(hmbz), and $^4A''/^3A''$ for Co/Co$^+$(hmbz). In these high-spin states, the aromatic ring remains nearly planar. This finding is in contrast to the previous study of Sc(hmbz), for which low-spin states were identified and the aromatic ring was severely distorted.

## ■ ASSOCIATED CONTENT

**Supporting Information.** A table of the geometries of hexamethylbenzene and M(hexamethylbenzene) (M = Sc, Ti, V, and Co) from DFT/B3LYP calculations. This material is available free of charge via the Internet at http://pubs.acs.org.

## ■ AUTHOR INFORMATION

**Corresponding Author**
*E-mail:dyang0@uky.edu.

## ■ ACKNOWLEDGMENT

We are grateful for the financial support from the National Science Foundation Division of Chemistry. We also acknowledge additional support from donors of the Petroleum Research Fund of the American Chemical Society and Kentucky Science and Engineering Foundation.

## ■ REFERENCES

(1) Jun, C.-H. *Chem. Soc. Rev.* **2004**, *33*, 610.
(2) Jones, W. D.; Feher, F. J. *J. Am. Chem. Soc.* **1982**, *104*, 4240.
(3) Jones, W. D.; Feher, F. J. *J. Am. Chem. Soc.* **1984**, *104*, 4240.
(4) Muetterties, E. L.; Bleeke, J. R. *Acc. Chem. Res.* **1979**, *12*, 324.
(5) Bleeke, J. R.; Muetterties, E. L. *J. Am. Chem. Soc.* **1981**, *103*, 556.
(6) Steffey, B. D.; Chesnut, R. W.; Kerschner, J. L.; Pellechia, P. J.; Fanwick, P. E.; Rothwell, I. P. *J. Am. Chem. Soc.* **1989**, *111*, 378.
(7) Duncan, M. A. *Int. J. Mass Spectrom.* **2008**, *272*, 99.
(8) Lyon, J. T.; Andrews, L. *J. Phys. Chem. A* **2006**, *110*, 7806.
(9) Ouhlal, A.; Selmani, A.; Yelon, A. *Chem. Phys. Lett.* **1995**, *243*, 269.
(10) Pandey, R.; Rao, B. K.; Jena, P.; Blanco, M. A. *J. Am. Chem. Soc.* **2001**, *123*, 3799.

(11) Kurikawa, T.; Takeda, H.; Hirano, M.; Judai, K.; Arita, T.; Nagao, S.; Nakajima, A.; Kaya, K. *Organometallics* **1999**, *18*, 1430.
(12) Chaquin, P.; Costa, D.; Lepetit, C.; Che, M. *J. Phys. Chem. A* **2001**, *105*, 4541.
(13) Imura, K.; Ohoyama, H.; Kasai, T. *Chem. Phys. Lett.* **2003**, *369*, 55.
(14) Pandey, R.; Rao, B. K.; Jena, P.; Newsam, J. M. *Chem. Phys. Lett.* **2000**, *321*, 142.
(15) Li, H. Y.; Li, C. P.; Fan, H. W.; Yang, J. C. *J. Mol. Struct.: THEOCHEM* **2010**, *952*, 67.
(16) Zheng, W. J.; Nilles, J. M.; Thomas, O. C.; Bowen, K. H. *Chem. Phys. Lett.* **2005**, *401*, 266.
(17) Andrews, M. P.; Huber, H. X.; Mattar, S. M.; Mcintosh, D. F.; Ozin, G. A. *J. Am. Chem. Soc.* **1983**, *105*, 6170.
(18) Andrews, M. P.; Mattar, S. M.; Ozin, G. A. *J. Phys. Chem.* **1986**, *90*, 744.
(19) Kandalam, A. K.; Rao, B. K.; Jena, P.; Pandey, R. *J. Chem. Phys.* **2004**, *120*, 10414.
(20) Lyon, J. T.; Andrews, L. *J. Phys. Chem. A* **2005**, *109*, 431.
(21) Mattar, S. M.; Sammynaiken, R. *J. Chem. Phys.* **1997**, *106*, 1080.
(22) Zhang, X. Y.; Wang, J. L. *J. Phys. Chem. A* **2008**, *112*, 296.
(23) Bauschlicher, C. W.; Partridge, H.; Langhoff, S. R. *J. Phys. Chem.* **1992**, *96*, 3273.
(24) Yang, C. N.; Klippenstein, S. J. *J. Phys. Chem. A* **1999**, *103*, 1094.
(25) Klippenstein, S. J.; Yang, C. N. *Int. J. Mass Spectrom.* **2000**, *201*, 253.
(26) Jaeger, T. D.; van Heijnsbergen, D.; Klippenstein, S. J.; von Helden, G.; Meijer, G.; Duncan, M. A. *J. Am. Chem. Soc.* **2004**, *126*, 10981.
(27) Weis, P.; Kemper, P. R.; Bowers, M. T. *J. Phys. Chem. A* **1997**, *101*, 8207.
(28) Jaeger, T. D.; Pillai, E. D.; Duncan, M. A. *J. Phys. Chem. A* **2004**, *108*, 6605.
(29) van Heijnsbergen, D.; von Helden, G.; Meijer, G.; Maitre, P.; Duncan, M. A. *J. Am. Chem. Soc.* **2002**, *124*, 1562.
(30) Lee, J. S.; Lei, Y. X.; Kumari, S.; Yang, D. S. *J. Phys. Chem. A* **2010**, *114*, 9136.
(31) Sohnlein, B. R.; Li, S. G.; Fuller, J. F.; Yang, D. S. *J. Chem. Phys.* **2005**, *123*, 014318.
(32) Proch, D.; Trickl, T. *Rev. Sci. Instrum.* **1989**, *60*, 713.
(33) Moore, C. E. *Atomic Energy Levels*; National Bureau of Standards: Washington, DC, 1971.
(34) Duncan, M. A.; Dietz, T. G.; Smalley, R. E. *J. Chem. Phys.* **1981**, *75*, 2118.
(35) Krasnokutski, S. A.; Lei, Y. X.; Lee, J. S.; Yang, D. S. *J. Chem. Phys.* **2008**, *129*, 124309.
(36) Rothman, L. S.; Jacquemart, D.; Barbe, A.; Benner, D. C.; Birk, M.; Brown, L. R.; Carleer, M. R.; Chackerian, C.; Chance, K.; Coudert, L. H.; Dana, V.; Devi, V. M.; Flaud, J. M.; Gamache, R. R.; Goldman, A.; Hartmann, J. M.; Jucks, K. W.; Maki, A. G.; Mandin, J. Y.; Massie, S. T.; Orphal, J.; Perrin, A.; Rinsland, C. P.; Smith, M. A. H.; Tennyson, J.; Tolchenov, R. N.; Toth, R. A.; Vander Auwera, J.; Varanasi, P.; Wagner, G. *J. Quant. Spectrosc. Radiat. Transfer* **2005**, *96*, 139.
(37) Frisch, M. J.; Trucks, G. W.; Schlegel, H. B.; Scuseria, G. E.; Robb, M. A.; Cheeseman, J. R.; Montgomery, J. J. A.; Vreven, T.; Kudin, K. N.; Burant, J. C.; Millam, J. M.; Iyengar, S. S.; Tomasi, J.; Barone, V.; Mennucci, B.; Cossi, M.; Scalmani, G.; Rega, N.; Petersson, G. A.; Nakatsuji, H.; Hada, M.; Ehara, M.; Toyota, K.; Fukuda, R.; Hasegawa, J.; Ishida, M.; Nakajima, T.; Honda, Y.; Kitao, O.; Nakai, H.; Klene, M.; Li, X.; Knox, J. E.; Hratchian, H. P.; Cross, J. B.; Bakken, V.; Adamo, C.; Jaramillo, J.; Gomperts, R.; Stratmann, R. E.; Yazyev, O.; Austin, A. J.; Cammi, R.; Pomelli, C.; Ochterski, J. W.; Ayala, P. Y.; Morokuma, K.; Voth, G. A.; Salvador, P.; Dannenberg, J. J.; Zakrzewski, V. G.; Dapprich, S.; Daniels, A. D.; Strain, M. C.; Farkas, O.; Malick, D. K.; Rabuck, A. D.; Raghavachari, K.; Foresman, J. B.; Ortiz, J. V.; Cui, Q.; Baboul, A. G.; Clifford, S.; Cioslowski, J.; Stefanov, B. B.; Liu, G.; Liashenko, A.; Piskorz, P.; Komaromi, I.; Martin, R. L.; Fox, D. J.; Keith, T.; Al-Laham, M. A.; Peng, C. Y.; Nanayakkara, A.; Challacombe, M.; Gill, P. M. W.; Johnson, B.; Chen, W.; Wong, M. W.; Gonzalez, C.; Pople, J. A. *Gaussian 03*; Gaussian, Inc: Wallingford, CT, 2004.
(38) Sohnlein, B. R.; Li, S.; Yang, D. S. *J. Chem. Phys.* **2005**, *123*, 214306.
(39) Sohnlein, B. R.; Fuller, J. F.; Yang, D. S. *J. Am. Chem. Soc.* **2006**, *128*, 10692.
(40) Sohnlein, B. R.; Lei, Y. X.; Yang, D. S. *J. Chem. Phys.* **2007**, *127*, 114302.
(41) Lee, J. S.; Lei, Y. X.; Kumari, S.; Yang, D. S. *J. Chem. Phys.* **2009**, *131*, 104304.
(42) Lee, J. S.; Kumari, S.; Yang, D. S. *J. Phys. Chem. A* **2010**, *114*, 11277.
(43) Zhang, C. H.; Krasnokutski, S. A.; Zhang, B.; Yang, D. S. *J. Chem. Phys.* **2009**, *131*, 054303.
(44) Yang, D. S.; Zgierski, M. Z.; Rayner, D. M.; Hackett, P. A.; Martinez, A.; Salahub, D. R.; Roy, P. N.; Carrington, T. *J. Chem. Phys.* **1995**, *103*, 5335.
(45) Berces, A.; Zgierski, M. Z.; Yang, D.-S. *Computational Molecular Spectroscopy*; Wiley: New York, 2000.
(46) Duschinsky, F. *Acta Physicochim. URSS* **1937**, *7*, 551.
(47) *NIST Standard Reference Database 69*. http://webbook.nist.gov/chemistry/ (accessed 2009).
(48) Hamilton, W. C.; Edmonds, J. W.; Tippe, A.; Rush, J. J. *Discuss. Faraday Soc.* **1969**, *48*, 192.
(49) Maverick, E.; Trueblood, K. N.; Bekoe, D. A. *Acta Crystallogr., Sect. B* **1978**, *34*, 2777.
(50) Melissas, V.; Faegri, K.; Almlof, J. *J. Am. Chem. Soc.* **1985**, *107*, 4640.
(51) Arney, D. J.; Wexler, P. A.; Wigley, D. E. *Organometallics* **1990**, *9*, 1282.
(52) Fuller, J. F.; Li, S. G.; Sohnlein, B. R.; Rothschopf, G. K.; Yang, D. S. *Chem. Phys. Lett.* **2002**, *366*, 141.
(53) Sawka-Dobrowolska, W.; Bator, G.; Sobczyk, L.; Pawlukojc, A.; Ptasiewicz-Bak, H.; Rundlof, H.; Krawczyk, J.; Nowina-Konopka, M.; Jagielski, P.; Janik, J. A.; Prager, M.; Steinsvoll, O.; Grech, E.; Nowicka-Scheibe, J. *J. Chem. Phys.* **2005**, 123.
(54) Lide, D. R. *CRC Handbook of Chemistry and Physics*, 88 ed.; CRC Press: Boca Raton, FL, 2008.
(55) Yang, D. S. *J. Phys. Chem. Lett.* **2011**, *2*, 25.